AGU PUBLICATIONS

Geophysical Research Letters

RESEARCH LETTER
10.1002/2014GL060310

Key Points:
- Rover landing and descent stage crash sites consistent with dusty basalt
- Hydroxylated silica detected in nearby light-toned terrain
- Dunes exhibit variable olivine and pyroxene content according to morphology

Correspondence to:
S. L. Murchie,
Scott.Murchie@jhuapl.edu

Citation:
Seelos, K. D., F. P. Seelos, C. E. Viviano-Beck, S. L. Murchie, R. E. Arvidson, B. L. Ehlmann, and A. A. Fraeman (2014), Mineralogy of the MSL Curiosity landing site in Gale crater as observed by MRO/CRISM, *Geophys. Res. Lett.*, *41*, 4880–4887, doi:10.1002/2014GL060310.

Received 23 APR 2014
Accepted 3 JUL 2014
Accepted article online 8 JUL 2014
Published online 23 JUL 2014

Mineralogy of the MSL Curiosity landing site in Gale crater as observed by MRO/CRISM

Kimberly D. Seelos[1], Frank P. Seelos[1], Christina E. Viviano-Beck[1], Scott L. Murchie[1], Raymond E. Arvidson[2], Bethany L. Ehlmann[3], and Abigail A. Fraeman[2]

[1]Applied Physics Laboratory, Johns Hopkins University, Laurel, Maryland, USA, [2]Department of Earth and Planetary Sciences, Washington University, St. Louis, Missouri, USA, [3]Division of Geological and Planetary Sciences, California Institute of Technology, Pasadena, California, USA

Abstract Orbital data acquired by the Compact Reconnaissance Imaging Spectrometer for Mars (CRISM) and High Resolution Imaging Science Experiment instruments on the Mars Reconnaissance Orbiter (MRO) provide a synoptic view of compositional stratigraphy on the floor of Gale crater surrounding the area where the Mars Science Laboratory (MSL) Curiosity landed. Fractured, light-toned material exhibits a 2.2 μm absorption consistent with enrichment in hydroxylated silica. This material may be distal sediment from the Peace Vallis fan, with cement and fracture fill containing the silica. This unit is overlain by more basaltic material, which has 1 μm and 2 μm absorptions due to pyroxene that are typical of Martian basaltic materials. Both materials are partially obscured by aeolian dust and basaltic sand. Dunes to the southeast exhibit differences in mafic mineral signatures, with barchan dunes enhanced in olivine relative to pyroxene-containing longitudinal dunes. This compositional difference may be related to aeolian grain sorting.

1. Introduction

On 6 August 2012, the Mars Science Laboratory (MSL) rover, Curiosity, successfully landed on the floor of Gale crater in an area that once had flowing water on the surface [*Williams et al.*, 2013]. The landing site was chosen because of its proximity to a mound of layered sediments, named Aeolis Mons and informally called Mount Sharp, that is thought to record a changing aqueous environment [*Grotzinger et al.*, 2012]. Layers consisting of clay-bearing sediments, which may indicate neutral pH, are overlain by sulfate-rich sediments which suggest a drier and more acidic, saline environment [*Milliken et al.*, 2010].

The Mars Reconnaissance Orbiter (MRO) acquired high-resolution images covering the landing site to determine the geologic context of Curiosity's measurements and to assist in planning its field traverses. This paper describes mineral signatures on the floor of Gale crater surrounding MSL's landing site, as measured by MRO's Compact Reconnaissance Imaging Spectrometer for Mars (CRISM). We include data acquired both prior to landing and in January 2013, just after landing, that show the blast zones partially cleaned of loosely adhering dust by the retrorockets of the MSL "sky crane" descent system (Figure 1).

2. Background

2.1. MSL Landing Site

The Curiosity landing site is located at 4.59°S, 137.44°E, at the distal end of the Peace Vallis alluvial fan system on the floor of Gale crater [*Palucis et al.*, 2013]. The early part of the landed mission focused on characterizing the morphology and mineralogy of these fan deposits, prior to driving toward the base of the 5.5 km high stack of layered materials forming the central sedimentary mound called Mount Sharp [*Grotzinger*, 2013]. Remote sensing data suggest that these layers contain phyllosilicates, sulfates, and iron oxide minerals formed through some combination of fluvial, lacustrine, and aeolian processes [*Milliken et al.*, 2010; *Thomson et al.*, 2011; *Kite et al.*, 2013; *Fraeman et al.*, 2013a]. The sequence of beds in this stack may preserve a paleoclimatic transition from the more pH-neutral conditions on early Mars to the dryer, acidic conditions that dominated later in Mars' history and persist to present day [*Bibring et al.*, 2006]. To reach these altered layered materials, Curiosity must also navigate through a large dune field that surrounds Mount Sharp [*Fraeman et al.*, 2013b; *Silvestro et al.*, 2013] that is composed of basaltic sand [*Rogers and Bandfield*, 2009; *Lane and Christensen*, 2013].

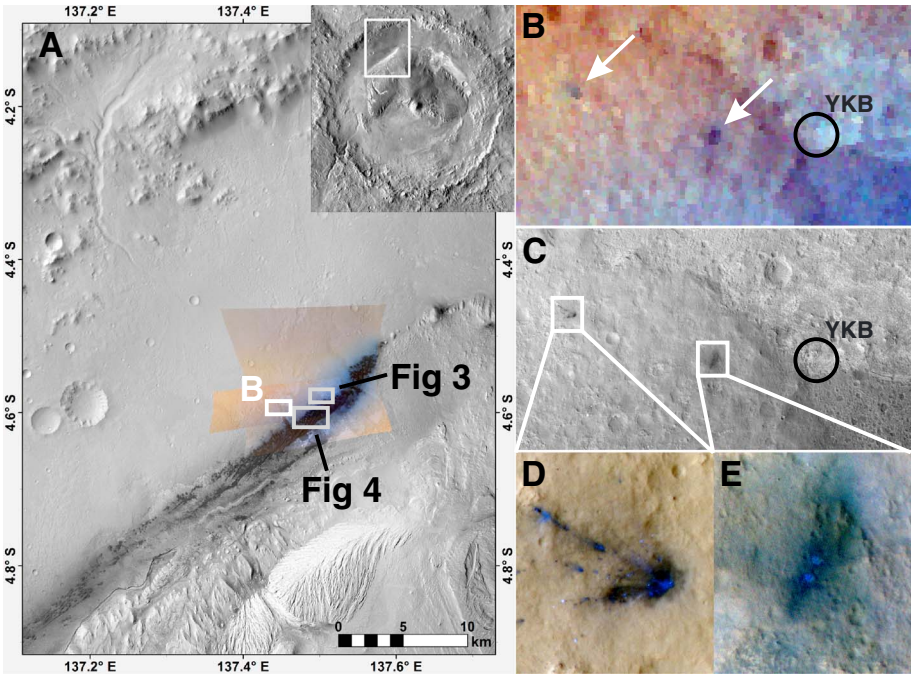

Figure 1. Gale crater context. (a) CRISM images FRT0002037A and FRS00028346 are rendered as visible red-green-blue composites and overlain on a CTX mosaic of the MSL landing site and field area. Locations of Figures 1b, 3, and 4 are labeled, and the inset shows the location within Gale crater. (b) Enhanced color CRISM image (FRS00028346) with the landing site scour zone and descent stage crash sites discernable as dark spots (arrows). The location of Yellowknife Bay (YKB) is also indicated. (c) HiRISE image ESP_030313_1755 of the same area as Figure 1b. (d, e) Enlargements of the decent stage crash site and thruster scour marks as observed in enhanced HiRISE color (ESP_28612_1755 and ESP_030313_1755, respectively). Image subsets are 125 m across.

The selection of Curiosity's landing site was enabled by the remote sensing instruments onboard several orbital platforms, including MRO which carries the Context Imager (CTX) [*Malin et al.*, 2007], High Resolution Imaging Science Experiment (HiRISE) [*McEwen et al.*, 2007], and CRISM [*Murchie et al.*, 2007] instruments. CRISM is used to determine the minerals present at the surface, which helps to detect distinctive geologic units and assess the nature of past aqueous environments. HiRISE and CTX provide morphologic information regarding the minerals' stratigraphic context while also addressing landing site safety concerns including the presence and distribution of boulders and steep slopes. Joint analysis of all three data sets helps to develop detailed hypotheses that the rover tests during its mission [e.g., *Milliken et al.*, 2010; *Thomson et al.*, 2011] and to put the landed measurements into geologic context.

2.2. CRISM Data Properties and Processing

In CRISM's full-resolution observing mode (i.e., observations prefaced with "FRT" or "FRS"), data are acquired in 544 visible through short-wave infrared wavelengths (0.4–3.9 μm) at 6.55 nm spectral sampling and ~18 m/pixel spatial sampling. This spectral range enables identification of common iron-bearing minerals as well as products of aqueous alteration, including hydrated sulfates and silica, phyllosilicates, and carbonates. Prior to analysis, CRISM data are radiometrically calibrated to I/F (radiance coefficient), then processed through a series of procedures to correct I/F to what would be observed at a near-nadir geometry with normal illumination and without atmospheric gases. From these data, georeferenced maps of mineralogically distinctive units are produced. The procedures applied include the following: (1) standard photometric and atmospheric corrections [*Murchie et al.*, 2009; *Morgan et al.*, 2011], (2) empirical correction for along-track variability due to the instrument's gimbal motion and aerosol scattering as a function of atmospheric path length [*Seelos et al.*, 2011, 2012], (3) empirical correction for cross-track spectral variation due to spectral smile [*Seelos et al.*, 2011, 2012], (4) reduction of spectral variability to a series of spectral "summary parameters" [*Pelkey et al.*, 2007; *Viviano-Beck et al.*, 2014], and (5) map projection.

Table 1. Source Descriptions for CRISM Spectra[a]

Numerator and Denominator Spectra	CRISM Image ID	Location[b] (*X*, *Y*)	Location[b] (°N, °E)	# Pixels
Descent stage crash site (num)	FRS00028346	383, 94	−4.589, 137.417	9 (3 × 3 avg)
Descent stage crash site (den)	FRS00028346	383, 153	−4.573, 137.434	15 (15 × 1 avg)
Landing site scour zone (num)	FRS00028346	348, 76	−4.593, 137.445	9 (3 × 3 avg)
Landing site scour zone (den)	FRS00028346	348, 166	−4.569, 137.443	9 (3 × 3 avg)
Light-toned material (num)	FRS00028346	130, 92	−4.580, 137.507	9 (3 × 3 avg)
Light-toned material (den)	FRS00028346	130, 172	−4.560, 137.504	9 (3 × 3 avg)
Light-toned material (num)	FRT0000C518	397, 403	−4.577, 137.508	11 (ROI[c])
Light-toned material (den)	FRT0000C518	397, 442	−4.553, 137.505	15 (ROI[c])
HCP-enriched dunes (num)	FRT0000C518	592, 252	−4.639, 137.461	15 (ROI[c])
HCP-enriched dunes (den)	FRT0000C518	592, 430	−4.570, 137.441	20 (ROI[c])
Olivine-enriched dunes (num)	FRT0000C518	491, 301	−4.622, 137.487	35 (ROI[c])
Olivine-enriched dunes (den)	FRT0000C518	493, 436	−4.562, 137.473	43 (ROI[c])

[a]num = Numerator, den = Denominator, avg = Average.
[b](*X*, *Y*) pixel coordinates extracted from the unprojected CRISM L-detector Targeted Reduced Data Record (TRDR); latitude (°N) and longitude (°E) coordinates are planetocentric, positive east and International Astronomical Union 2000 standard and extracted from the unprojected CRISM L-detector Derived Data Record (DDR). Coordinates may not precisely align with other data sets.
[c]ROI = Region of interest; often irregularly shaped cluster(s) of pixels, center locations provided.

CRISM observations discussed here include FRT0000C518 which was acquired on 3 September 2008, prior to MSL's landing, and FRS00028346 acquired on 13 January 2013, just a few months after MSL landed in Gale crater. HiRISE images acquired contemporaneously with the CRISM images (PSP_009861_1755 and ESP_030313_1755, respectively) and previously (ESP ESP_28612_1755 and ESP_024023_1755) provide regional morphologic context along with previously acquired CTX images that have been rendered into a mosaic.

CRISM images acquired prior to landing were analyzed to search for mineral signatures. Spectral summary parameters, which quantify the strengths of absorptions due to key mineral phases, enabled localization of the strongest signatures of the major minerals present. The most useful parameters used were those designed to detect olivine (OLINDEX3), high-calcium pyroxene (HCPINDEX2), ferric minerals in dust (BD530), and hydrated silica (MIN2250); these all use the formulations of *Viviano-Beck et al*. [2014]. In order to reduce noise in spectra extracted from the regions with the strongest signatures, several (9–43) pixels corresponding to locations exhibiting the highest parameter values were averaged together (Table 1). In addition, we extracted spectra from postlanding images of the landing site scour zone and the descent stage crash site (Figure 1b) to provide insight into the properties of the relatively dust-free substrate regolith. For each extracted spectrum of interest, a relatively bland spectrum was collected and averaged from a nearby area that lies in the same detector column(s); the bland spectrum was then used as a denominator in a ratio calculation to emphasize the unique spectral characteristics of the material of interest. Each denominator spectrum is from a dust-dominated location; thus, the resulting ratio spectra highlight absorptions relative to dust.

3. Results and Discussion

Three categories of nondust-dominated materials were found at or near the MSL landing site: (1) materials at the landing and descent stage crash sites, which are most consistent with basaltic material coated or spatially mixed with dust, (2) nearby light-toned material that exhibits spectral signatures consistent with hydroxylated silica, and (3) the circum-Mount Sharp dune field where longitudinal and barchan dunes show enhancement in signatures from pyroxene and olivine, respectively (Figure 2). The spectral properties and geomorphic setting for each of these materials are discussed below. The dust itself is consistent with that observed elsewhere [e.g., *Morris et al*., 2001], having a red slope and shallow 0.53 μm absorption at visible wavelengths due to nanophase iron oxide, a broad, shallow 1 μm absorption consistent with fine-grained olivine and pyroxene, and a deep 3 μm absorption due to molecular water but no other confirmed mineralogic signatures in CRISM data.

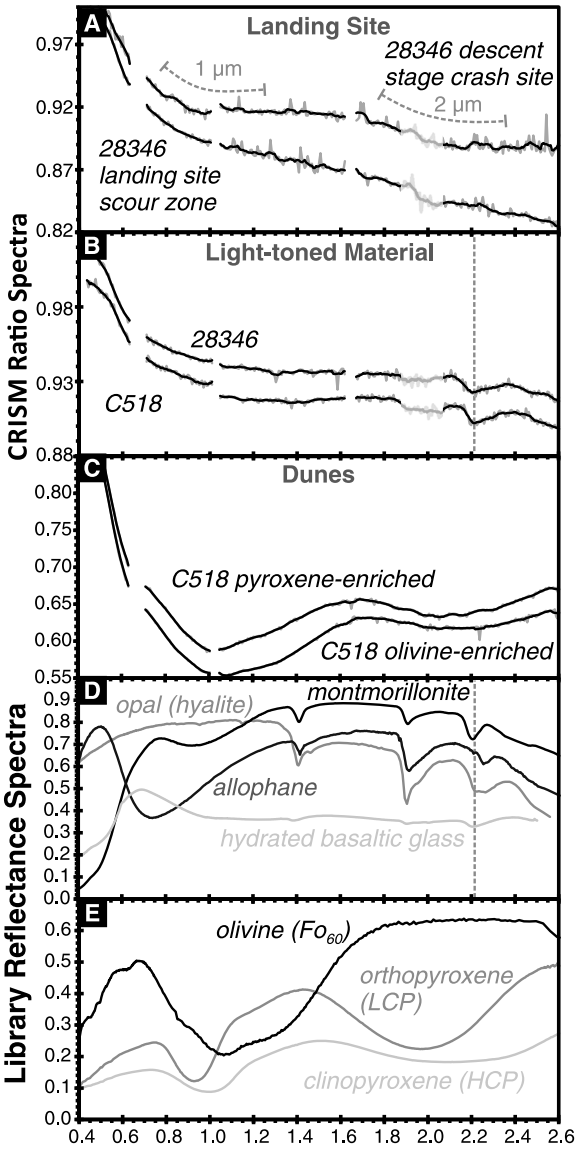

Figure 2. CRISM spectra of the (a) MSL landing and descent stage crash sites, (b) nearby light-toned terrain, and (c) dunes. Each spectrum represents an average of several pixels from FRS00028346 or FRT0000C518 that has been normalized to an in-column spectrum of a more spectrally neutral, dusty area to emphasize spectral features (Table 1). For each spectrum, the gray line is the original ratio, while the black line is smoothed by taking the average of the seven nearest spectral data points. The wavelength range near 2 μm is masked in Figures 2a and 2b because of noise and residuals in the atmospheric correction. Curved dashed lines in Figure 2a mimic the broad 1 and 2 μm absorptions, and a vertical dashed line in Figure 2b indicates the band minimum located at 2.23 μm. (d) Library spectra of common minerals having an absorption near 2.2 μm, including montmorillonite 1292 F35[1], opal TM8896 (hyalite)[2], allophane LAAL02[1] (shown offset by 0.05), and hydrated basaltic glass[3] (shown amplified by five). The vertical dashed line is at the same wavelength position as in Figure 2b to facilitate comparison. (e) Library spectra of mafic minerals, including olivine KI3189 Fo60[2], orthopyroxene CASB52[1], and clinopyroxene/augite C1PP49[1]. The Fo60 olivine library spectrum was selected to best match the results presented in *Lane and Christensen* [2013]. Library spectra are available at (1) the Planetary Data System (PDS) (http://speclib.rsl.wustl.edu/), (2) U.S. Geological Survey (http://speclab.cr.usgs.gov/spectral-lib.html), or (3) from *Swayze et al.* [2007].

3.1. Landing Site

The final stage of MSL's entry, descent, and landing [*Steltzner et al.*, 2006] phase involved the descent stage "sky crane" firing its two thrusters, stabilizing midair, and lowering the Curiosity rover via a tether to the Martian surface. The Mars Descent Imager [*Malin et al.*, 2009] camera recorded a billowing of dust [*Schieber et al.*, 2013]; sand to small pebble-sized grains observed on the rover deck after landing provided further evidence for significant scouring of the local surface. These observations were corroborated by a postlanding HiRISE image that revealed a distinct darkening of the surface, most prominently in two circular patches directly under the thrusters but also more diffusely in the surrounding ~50 × 100 m region (Figures 1c and 1e). After the rover touched down, the tether was released and the descent stage executed a preprogrammed command sequence to fly off and crash into the surface at a safe distance [*Grotzinger et al.*, 2012]. The crash site is also easily discernable in postlanding HiRISE images as a radiating distribution of debris, generally low in albedo but including dark rays and small bright fragments of spacecraft hardware (Figures 1c and 1d). The crash site is comparable in area to the landing site, and both were large enough for CRISM to resolve (Figure 1b). Remote analysis of the visible/near-infrared spectral properties and mineralogy of the underlying, relatively dust-free surfaces at these locations was made possible by the nature of Curiosity's landing that provided windows through the dust cover.

The landing site scour zone and descent stage crash site (Figure 2a) exhibit a lesser Fe^{3+} absorption near 0.53 μm due to nanophase ferric oxide than unscoured surfaces. At 0.7–2.5 μm where unratioed spectral slopes are generally neutral, they exhibit a relatively negative spectral slope toward longer wavelengths as compared to dust, and enhanced Fe^{2+} absorptions centered near ~1 and 2 μm in the case of the

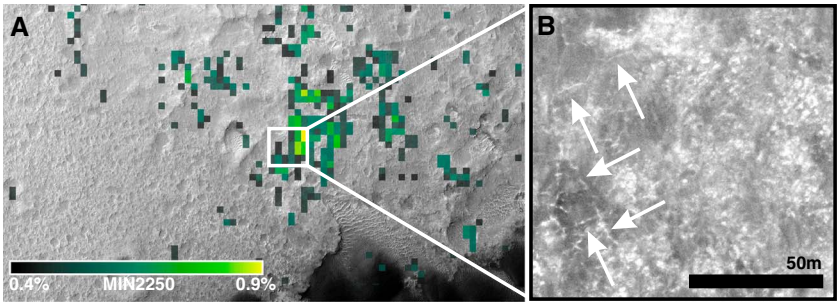

Figure 3. Morphologic context of material with a 2.2 μm absorption. (a) Summary parameter MIN2250 [*Viviano-Beck et al*., 2014] shows strength of the broad 2.2 μm absorption interpreted to be due to hydroxylated silica overlain on HiRISE image PSP_009861_1755. (b) Stronger spectral signatures are associated with polygonally fractured light-toned terrain in the eastern portion of the image. A loosely interconnected series of submeter-wide lineaments (white arrows), located just west of the strongest 2.2 μm signal, may represent erosion-resistant filled fractures.

descent stage crash site spectrum. The negative slope is absent from ratio spectra of nearby dunes. The lesser 0.53 μm absorption and negative infrared slope are consistent with the direct observations of dust removal during landing. Martian dust exhibits a neutral or positive infrared slope, whereas a residual dust coating on a scoured basaltic substrate exhibits a negative slope [*Fischer and Pieters*, 1993]. At the descent stage crash site, subtle broad ~1 and 2 μm features are also apparent and consistent with an increase in content of the mafic minerals olivine and pyroxene at the optical surface. However, the absorptions are not strong enough to distinguish between high- and low-calcium pyroxene (e.g., Figure 2e). The fact that both absorptions are apparent at the crash site and not the landing site scour zone possibly indicates that greater dust removal or deeper excavation occurred at the crash site and/or over a larger area. However, the pyroxene spectral signature of the substrate at the crash site is consistent with the dominant basaltic component of the soil as determined by X-ray diffraction results from the MSL Chemistry and Mineralogy instrument [*Bish et al*., 2013; *Blake et al*., 2013] at the landing site.

3.2. Light-Toned Material

High-resolution geomorphic mapping of the landing site and surrounding region has identified several areas of fractured, light-toned, coherent material [*Sumner et al*., 2013]. This light-toned unit is interpreted as occurring stratigraphically beneath basaltic material exposed at the rover landing and descent stage crash sites, possibly forming a horizontal extension of material at the toe of the Peace Vallis fan to the northwest, and probably is fluvial in origin [*Sumner et al*., 2013]. In CRISM scenes covering similar light-toned outcrops, some exposures exhibit a weak but spatially coherent ~2.2 μm absorption (Figures 2b and 3). Mineral absorptions centered at this wavelength (Figure 2d) can be caused by hydroxyl ions bound to aluminum (Al-OH) in Al-bearing phyllosilicates. Hydroxyl bound to silica (Si-OH) in opal, hydrated glass, and other noncrystalline or poorly crystalline aluminosilicates also causes a feature near this wavelength, but it is distinguishable from that caused by crystalline Al-OH-bearing minerals based on spectral shape and width [e.g., *Swayze et al*., 2007; *Milliken et al*., 2008]. In crystalline and/or well-hydrated materials, distinct ~1.4 and ~1.9 μm molecular and bound water absorptions are also present. Fe-bearing minerals such as dust or rock coatings can often dominate absorptions shortward of 2 μm making the 1.4 μm feature weak or absent in Martian mineral spectra. These materials become more transparent at longer wavelengths, allowing the 1.9 μm absorption to be seen [*Swayze*, 2004; *Cloutis et al*., 2006]; however, the 1.9 μm absorption can also be obscured by spectral noise and residuals from the atmospheric correction, as it overlaps with the dominant atmospheric CO_2 bands. Hints of a 1.9 μm feature are present in the light-toned material spectra (Figure 2b), but the 1.9 μm band is not reproducible convincingly (present within multiple scenes) above the level of noise. Thus, we interpret the center and width of the 2.2 μm absorption in the light-toned material and the lack of diagnostic water bands near 1.4 and 1.9 μm to be most consistent with hydroxylated silica either in hydrated basaltic glass or in opaline silica (hyalite) that has been partially dehydrated, with molecular water largely removed but hydroxyl retained (Figure 2d).

The presence of hydroxylated silica in the light-toned fractured material is consistent with several independent observations. The light-toned material is partially and variably covered by a lower albedo

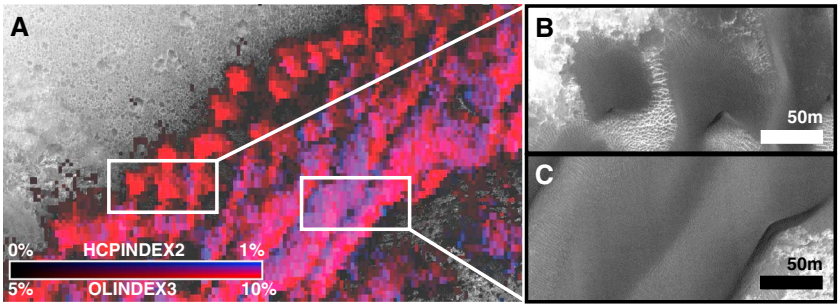

Figure 4. Dune mineralogy and morphology. (a) Summary parameters OLINDEX3 and HCPINDEX2 [*Viviano-Beck et al.*, 2014] from CRISM image FRT0000C815 are shown as red and blue images planes, respectively, and are overlain on HiRISE image ESP_024023_1755. Red pixels corresponding to greater relative spectral contribution of olivine are primarily on (b) the barchan dunes, whereas blue-purple pixels highlight a greater high-calcium pyroxene (HCP) contribution are primarily on (c) the longitudinal dunes.

smooth material, possibly basaltic sand. In areas where this cover material is more continuous a series of light-toned, narrow, rectilinearly to polygonally arranged ridges are highlighted (Figure 3b). While the 2.2 μm signal is strongest in the adjacent area to the east where there is greater exposure of light-toned terrain, the proximity of these ridges, which are only observed in this area at this spatial scale, suggests a genetic relationship. Similar positive relief ridges at a variety of scales at various landing sites on Mars have been interpreted to form from erosion-resistant vein fill including but not restricted to hydrated/hydroxylated silica [e.g., *Okubo and McEwen*, 2007; *Squyres et al.*, 2012; *Arvidson et al.*, 2014]. Occurrence of hydroxylated silica distal to the Peace Vallis fan deposit is also consistent with the work of *Carter et al.* [2013]. In their global examination of fan and deltaic deposits of varying sizes, they found that a distal annulus of hydrated silica is common on Mars. They interpret the silica likely to have formed by precipitation from aqueous solution. Here that precipitate may act as a cementing phase in basaltic sediments [*Vaniman et al.*, 2014].

The relationship of the hydroxylated silica to rocks and soils measured by Curiosity is unclear; the silica locality presented here is ~3 km away from the Yellowknife Bay sedimentary rocks explored by the rover, though perhaps within a similar geologic unit [*Sumner et al.*, 2013]. Yellowknife Bay mudstones analyzed with Curiosity's payload are chemically basaltic but with Mg-rich phyllosilicate (~20%), calcium sulfates (2–4%; anhydrite, bassanite), and a significant fraction of amorphous material (~30%) [*Vaniman et al.*, 2014; *McLennan et al.*, 2014]. If the volatile-rich amorphous component is derived from hydroxylated glass or poorly crystalline aluminosilicate, it would be consistent with the spectral signature observed by CRISM. However, there is little chemical difference between the composition of amorphous materials in Yellowknife Bay and in Rocknest sands [*Vaniman et al.*, 2014], which are considered representative of Gale crater floor sands, and the spatially extensive deposits of soils and sands within Gale do not exhibit a 2.2 μm feature in CRISM data. This implies that there is lateral variation in the mineralogy of the Yellowknife Bay and related distal Peace Vallis fan units. Silica precipitated from fluids [*McLennan*, 2003] or local aqueous alteration of the amorphous phase within the mudstones are two possible pathways that might have allowed for the formation of the distinctive 2.2 μm bearing light-toned material reported here.

3.3. Dunes

The light-toned unit and basaltic materials at the landing site are superposed by a dune field that circumscribes the west side of Mount Sharp (Figures 1a and 4). Ripples observed on the upper surface of these active longitudinal and barchan dunes [*Silvestro et al.*, 2013] show a modern dominant wind direction from the northeast. Both types of dunes show clear 1 μm and 2 μm absorptions due to pyroxene and olivine, presumably from a basaltic parent material (Figure 2c). However, in the barchan dunes, the 1 μm absorption is shifted to longer wavelengths with an increased inflection near 1.3 μm, consistent with presence of a greater fraction of olivine. In contrast, the longitudinal dunes exhibit enhanced and shorter wavelength positions of both the 1 and 2 μm bands that are consistent with a greater fraction of high-calcium pyroxene. The spatial distribution and concentration of these mafic minerals according to dune type is apparent in Figure 4.

Compositional differences between nearby Martian sand deposits have recently been recognized in a wide variety of locations on Mars. Differences in composition of sediment sources and aeolian separation of phases

having different densities are both thought to contribute to creating these differences [*Chojnacki et al*., 2014]. Here the close proximity and spectral similarity of the two dune types make different sediment sources unlikely. Instead, the relatively sediment-starved barchan dunes may be slightly enriched in larger or denser olivine-rich grains (specific gravity ~3.3, compared with ~2.9–3.0 for typical basalt) by deflation of lower density, more pyroxene-rich grains prevalent in the longitudinal dunes.

4. Conclusion

Orbital reconnaissance of the floor of Gale crater by the CRISM and HiRISE instruments on MRO provides an overview of compositional stratigraphy near the MSL landing site. Light-toned material identified as being enriched in hydroxylated silica phases may be distal sediment from the Peace Vallis fan and similar to the Yellowknife Bay unit explored by Curiosity. This material is overlain by more basaltic material, and both are partially obscured by surface dust and basaltic sand deposits. The active NE-SW trending dark dune field to the south and southeast of the landing site exhibits differences in mafic mineral signatures (i.e., olivine and high-calcium pyroxene) according to dune type that may be related to aeolian grain sorting. These observations based on orbital data serve as important context for Curiosity's in situ analyses and are readily testable as the rover continues its traverse toward Mount Sharp.

Acknowledgments

All data are publically available through the NASA Planetary Data System (PDS). We thank the MSL and MRO projects, the CRISM Science Operations Center, and the HiRISE Operations Center for collection and processing of the data shown here. We would also like to thank Melissa Lane and Brad Thomson for thoughtful reviews that improved the manuscript and Sheridan Ackiss for helping to finalize the manuscript.

The Editor thanks Bradley Thomson and Melissa Lane for their assistance in evaluating this paper.

References

Arvidson, R. E., et al. (2014), Ancient aqueous environments at Endeavour Crater, Mars, *Science*, *34*, doi:10.1126/science.1248097.

Bibring, J.-P., et al. (2006), Global mineralogical and aqueous Mars history derived from OMEGA/Mars Express data, *Science*, *312*, doi:10.1126/science.1122659.

Bish, D. L., et al. (2013), X-ray diffraction results from Mars Science Laboratory: Mineralogy of Rocknest at Gale Crater, *Science*, *341*, doi:10.1126/science.1238932.

Blake, D. F., et al. (2013), Curiosity at Gale Crater, Mars: Characterization and analysis of the Rocknest sand shadow, *Science*, *341*, doi:10.1126/science.1239505.

Carter, J., F. Poulet, J.-P. Bibring, N. Mangold, and S. Murchie (2013), Hydrous minerals on Mars as seen by the CRISM and OMEGA imaging spectrometers: Updated global view, *J. Geophys. Res. Planets*, *118*, 831–858, doi:10.1029/2012JE004145.

Chojnacki, M., D. M. Burr, J. E. Moersch, and J. J. Wray (2014), Valles Marineris dune sediment provenance and pathways, *Icarus*, *232*, 187–219, doi:10.1016/j.icarus.2014.01.011.

Cloutis, E. A., et al. (2006), Detection and discrimination of sulfate minerals using reflectance spectroscopy, *Icarus*, *184*, 121–157, doi:10.1016/j.icarus.2006.04.003.

Fischer, E., and C. M. Pieters (1993), The continuum slope of Mars: Bidirectional reflectance investigations and applications to Olympus Mons, *Icarus*, *102*, 185–202, doi:10.1006/icar.1993.1043.

Fraeman, A. A., et al. (2013a), A hematite-bearing layer in Gale Crater, Mars: Mapping and implications for past aqueous conditions, *Geology*, *41*, 1103–1106, doi:10.1130/G34613.1.

Fraeman, A. A., R. E. Arvidson, P. Bellutta, and R. S. Sletten (2013b) Climbing Mt. Sharp: Maximizing Curiosity's science over traversable terrains, *Eos Trans. AGU*, Fall Meet. Suppl., Abstract #P23B-1774.

Grotzinger, J. P. (2013), Analysis of surface materials by the Curiosity Mars rover, *Science*, *341*, 1475, doi:10.1126/science.1244258.

Grotzinger, J. P., et al. (2012), Mars Science Laboratory mission and science investigation, *Space Sci. Rev.*, *170*, 5–56, doi:10.1007/s11214-012-9892-2.

Kite, E. S., K. W. Lewis, M. P. Lamb, C. E. Newman, and M. I. Richardson (2013), Growth and form of the mound in Gale Crater, Mars: Slope wind enhanced erosion and transport, *Geology*, *41*, 543–546, doi:10.1130/G33909.1.

Lane, M. D., and P. R. Christensen (2013), Determining olivine composition of basaltic dunes in Gale Crater, Mars, from orbit: Awaiting ground truth from Curiosity, *Geophys. Res. Lett.*, *40*, 3517–3521, doi:10.1002/grl.50621.

Malin, M. C., et al. (2007), Context Camera investigation on board the Mars Reconnaissance Orbiter, *J. Geophys. Res.*, *112*, E05S04, doi:10.1029/2006JE002808.

Malin, M. C., M. A. Caplinger, K. S. Edgett, F. T. Ghaemi, M. A. Ravine, J. A. Schaffner, J. N. Maki, R. G. Willson, J. F. Bell III, and J. F. Cameron (2009), The Mars Science Laboratory (MSL) Mars Descent Imager (MARDI) flight instrument, paper presented at the 40th Lunar Planet. Sci. Conf., Lunar and Planetary Inst., The Woodlands, Tex., Abstract #1199.

McEwen, A. S., et al. (2007), Mars Reconnaissance Orbiter's High Resolution Imaging Science Experiment (HiRISE), *J. Geophys. Res.*, *112*, E05S02, doi:10.1029/2005JE002605.

McLennan, S. M. (2003), Sedimentary silica on Mars, *Geology*, *31*(4), 315–318.

McLennan, S. M., et al. (2014), Elemental geochemistry of sedimentary rocks at Yellowknife Bay, Gale Crater, Mars, *Science*, *343*, doi:10.1126/science.1244734.

Milliken, R., et al. (2008), Opaline silica in young deposits on Mars, *Geology*, *36*, 847–850, doi:10.1130/G24967A.1.

Milliken, R. E., J. P. Grotzinger, and B. J. Thomson (2010), Paleoclimate of Mars as captured by the stratigraphic record in Gale Crater, *Geophys. Res. Lett.*, *37*, L04201, doi:10.1029/2009GL041870.

Morgan, F., J. F. Mustard, S. M. Wiseman, F. P. Seelos, S. L. Murchie, P. C. McGuire, and the CRISM Team (2011), Improved algorithm for CRISM volcano scan atmospheric correction, paper presented at the 42nd Lunar Planet. Sci. Conf., Lunar and Planetary Inst., The Woodlands, Tex., Abstract #2453.

Morris, R. V., D. Golden, D. Ming, T. Shelfer, L. Jorgensen, J. Bell, T. Graff, and A. Mertzman, (2001), Phyllosilicate-poor palagonitic dust from Mauna Kea Volcano (Hawaii): A mineralogical analogue for magnetic Martian dust?, *J. Geophys. Res.*, *106*(E3), 5057–5083, doi:10.1029/2000JE001328.

Murchie, S., et al. (2007), Compact Reconnaissance Imaging Spectrometer for Mars (CRISM) on Mars Reconnaissance Orbiter (MRO), *J. Geophys. Res.*, *112*, E05S03, doi:10.1029/2006JE002682.

Murchie, S. L., et al. (2009), A synthesis of Martian aqueous mineralogy after 1 Mars year of observations from the Mars Reconnaissance Orbiter, *J. Geophys. Res.*, 114, E00D06, doi:10.1029/2009JE003342.

Okubo, C. H., and A. S. McEwen (2007), Fracture-controlled paleo-fluid flow in Candor Chasma, Mars, *Science*, *315*(5814), 983–985, doi:10.1126/science.1136855.

Palucis, M. C., W. E. Dietrich, A. G. Hayes, R. M. E. Williams, F. Calef, D. Y. Sumner, S. Gupta, C. J. Hardgrove, and the MSL Team (2013), Origin and evolution of the Peace Vallis fan system that drains into the Curiosity landing area, Gale Crater, paper presented at the 44th Lunar Planet. Sci. Conf., Lunar and Planetary Inst., The Woodlands, Tex., Abstract #1607.

Pelkey, S. M., et al. (2007), CRISM multispectral summary products: Parameterizing mineral diversity on Mars from reflectance, *J. Geophys. Res.*, *112*, E08S14, doi:10.1029/2006JE002831.

Rogers, A. D., and J. B. Bandfield (2009), Mineralogical characterization of Mars Science Laboratory candidate landing sites from THEMIS and TES data, *Icarus*, *203*, 437–453.

Schieber, J., M. C. Malin, T. S. Olson, F. Calef, K. Comeaux, and the MSL Science Team (2013), The final 2½ minutes of terror—What we learned about the MSL landing from the images taken by the MARDI descent imager, paper presented at the 44th Lunar Planet. Sci. Conf., Lunar and Planetary Inst., The Woodlands, Tex., Abstract #1260.

Seelos, F. P., S. L. Murchie, D. C. Humm, O. S. Barnouin, M. F. Morgan, H. W. Taylor, C. Hash, and the CRISM Team (2011), CRISM data processing and analysis products update—Calibration, correction, and visualization, paper presented at the 42nd Lunar Planet. Sci. Conf., Lunar and Planetary Inst., The Woodlands, Tex., Abstract #1438.

Seelos, F. P., M. F. Morgan, H. W. Taylor, S. L. Murchie, D. C. Humm, K. D. Seelos, O. S. Barnouin, C. E. Viviano, and the CRISM Team (2012), CRISM Map Projected Targeted Reduced Data Records (MTRDRs)—High level analysis and visualization data products, paper presented at Planetary Data: A Workshop for Users and Software Developers, U.S. Geol. Surv., Flagstaff, Ariz.

Silvestro, S., D. Vaz, R. C. Ewing, A. P. Rossi, L. K. Fenton, T. I. Michaels, J. Flahaut, and P. E. Geissler (2013), Pervasive aeolian activity along rover Curosity's traverse in Gale crater, Mars, *Geology*, *41*(4), 483–486, doi:10.1130/G34162.1.

Squyres, S. W., et al. (2012), Ancient impact and aqueous processes at Endeavour Crater, Mars, *Science*, *336*, doi:10.1126/science.1220476.

Steltzner, A., et al. (2006) Mars Science Laboratory entry, descent, and landing system, in *2006 IEEE Aerospace Conference*, Institute of Electrical and Electronics Engineers (IEEE), Piscataway, N. J., doi:10.1109/AERO.2006.1655796.

Sumner, D. Y., et al. (2013), Preliminary geological map of the Peace Vallis fan integrated with in situ mosaics from the Curiosity rover, Gale Crater, Mars, paper presented at the 44th Lunar Planet. Sci. Conf., Lunar and Planetary Inst., The Woodlands, Tex., Abstract #1699.

Swayze, G. A. (2004), Using reflectance spectroscopy to evaluate minerals of environmental concern, in *Infrared Spectroscopy in Exploration, Geochemistry and Remote Sensing, Short Course Ser.*, vol. 33, edited by P. L. King, M. S. Ramsey, and G. A. Swayze, pp. 181–196, Mineral. Assoc. of Can., Ottawa, Ont., Canada.

Swayze, G. A., R. E. Milliken, R. N. Clark, J. L. Bishop, B. L. Ehlmann, S. M. Pelke, J. F. Mustard, S. L. Murchie, and A. J. Brown, and the MRO CRISM Team (2007), Spectral evidence for hydrated volcanic and/or impact glass on Mars with MRO CRISM, paper presented at the 7th International Conf. on Mars, Lunar and Planetary Inst., Pasadena, Calif., Abstract #3384.

Thomson, B. J., N. T. Bridges, R. Milliken, A. Baldridge, S. J. Hook, J. K. Crowley, G. M. Marion, C. R. de Souza Filho, A. J. Brown, and C. M. Weitz (2011), Constraints on the origin and evolution of the layered mound in Gale Crater, Mars using Mars Reconnaissance Orbiter data, *Icarus*, *214*, 413–432, doi:10.1016/j.icarus.2011.05.002.

Vaniman, D. T., et al. (2014), Mineralogy of a mudstone at Yellowknife Bay, Gale Crater, Mars, *Science*, *343*, doi:10.1126/science.1243480.

Viviano-Beck, C. E., F. P. Seelos, et al. (2014), Revised CRISM spectral parameters and summary products based on the currently detected mineral diversity on Mars, *J. Geophys. Res. Planets*, *119*, 1403–1431, doi:10.1002/2014JE004627.

Williams, R. M. E., et al. (2013), Martian fluvial conglomerates at Gale Crater, *Science*, *340*, 1068–1072, doi:10.1126/science.1237317.